Geological Magazine

www.cambridge.org/geo

Original Article

Cite this article: Choudhary S, Sen K, Kumar S, Rana S, and Ghosh S (2021) Forsterite reprecipitation and carbon dioxide entrapment in the lithospheric mantle during its interaction with carbonatitic melt: a case study from the Sung Valley ultramafic–alkaline–carbonatite complex, Meghalaya, NE India. *Geological Magazine* **158**: 475–486. https://doi.org/10.1017/S0016756820000631

Received: 6 January 2020
Revised: 7 May 2020
Accepted: 20 May 2020
First published online: 20 August 2020

Keywords:
Fe-rich magnesite; metasomatism; forsterite; carbonatite; Raman spectroscopy; Kerguelen plume

Author for correspondence: Koushik Sen, Email: koushik.geol@gmail.com

CAMBRIDGE UNIVERSITY PRESS

Forsterite reprecipitation and carbon dioxide entrapment in the lithospheric mantle during its interaction with carbonatitic melt: a case study from the Sung Valley ultramafic–alkaline–carbonatite complex, Meghalaya, NE India

Shubham Choudhary[1], Koushik Sen[1], Santosh Kumar[2], Shruti Rana[1] and Swakangkha Ghosh[3]

[1]Wadia Institute of Himalayan Geology, 33 GMS Road, Dehradun-248001, India; [2]Department of Geology, Centre of Advanced Study, Kumaun University, Nainital, India and [3]North Eastern Space Applications Centre, Umiam, Meghalaya, India

Abstract

Carbonatite melts derived from the mantle are enriched in CO_2- and H_2O-bearing fluids. This melt can metasomatize the peridotitic lithosphere and liberate a considerable amount of CO_2. Experimental studies have also shown that a CO_2–H_2O-rich fluid can form Fe- and Mg-rich carbonate by reacting with olivine. The Sung Valley carbonatite of NE India is related to the Kerguelen plume and is characterized by rare occurrences of olivine. Our study shows that this olivine is resorbed forsterite of xenocrystic nature. This olivine bears inclusions of Fe-rich magnesite. Accessory apatite in the host carbonatite contains CO_2–H_2O fluid inclusions. Carbon and oxygen isotopic analyses indicate that the carbonatites are primary igneous carbonatites and are devoid of any alteration or fractionation. We envisage that the forsterite is a part of the lithospheric mantle that was reprecipitated in a carbonatite reservoir through dissolution–precipitation. Carbonation of this forsterite, during interaction between the lithospheric mantle and carbonatite melt, formed Fe-rich magnesite. CO_2–H_2O-rich fluid derived from the carbonatite magma and detected within accessory apatite caused this carbonation. Our study suggests that a significant amount of CO_2 degassed from the mantle by carbonatitic magma can become entrapped in the lithosphere by forming Fe- and Mg-rich carbonates.

1. Introduction

Primary carbonatite can form from different types of magma derived from the mantle, and it is suggested that partial melting, fractional crystallization or liquid immiscibility can generate distinct type of carbonatite magma (Mitchell, 2005). Carbonatite magma has very low viscosity; it migrates easily through the mantle and also reacts with it (Green & Wallace, 1988; Hammouda & Laporte, 2000). Carbonatitic magma in the mantle (including magnesio-carbonatites) reacts with depleted mantle wall rocks at < 2 GPa pressure and transforms into more calcite-rich composition with a high CaO/MgO content (Dalton & Wood, 1993). Experimental studies along with geochemical and mineralogical analyses of mantle xenoliths have shown that carbonate metasomatism can significantly alter the chemical properties of the lithospheric mantle (Green & Wallace, 1988; Yaxley *et al.* 1991, 1998; Hauri *et al.* 1993; Ionov *et al.* 1993; Boyd *et al.* 1997; Blundy & Dalton, 2000; Hammouda & Laporte, 2000; Kogarko *et al.* 2001; Dixon *et al.* 2008; Doucet *et al.* 2014; Pearson & Wittig, 2014; Pokhilenko *et al.* 2015; Sokol *et al.* 2016). Interaction of carbonatitic magma with mantle peridotite during carbonate metasomatism and the subsequent formation of olivine is well established (Green & Wallace, 1988; Dalton & Wood, 1993; Su *et al.* 2016). Carbonate metasomatism of dunite is a very fast process, where water and CO_2-bearing carbonatite magma can ascend through the lithospheric mantle by the dissolution of olivine and reprecipitation of forsterite (Hammouda & Laporte, 2000). This process alters a significant part of the lithospheric mantle with the fugitive CO_2 largely lost from the system (Yaxley, 1993). It can therefore be argued that carbonation of peridotitic lithosphere or CO_2 entrapment in the upper mantle by carbonate-rich melt is important in terms of global geodynamics, as it alters the physico-chemical properties of the upper mantle.

Here we report the occurrence of Fe-rich magnesite or (Fe, Mg)CO_3 as solid inclusions within a forsterite xenocryst from one carbonatite sample from the Sung Valley ultramafic–alkaline–carbonatite complex (UACC). This UACC is related to the Kerguelen plume activity (Veena *et al.* 1998). This carbonatite is primary igneous carbonatite (PIC) and has generated due to partial melting of carbonate peridotite in the mantle (Srivastava & Sinha, 2004).

This carbonatite interacted with the peridotitic lithosphere during ascent. Our objective was to assess the mineralogical changes this interaction has caused and also to understand the role of volatiles (CO_2 and H_2O) derived from the carbonatite in alteration of the peridotitic lithosphere. Our study shows carbonate metasomatism in the form of forsterite reprecipitation from olivine. This olivine was sourced from the peridotitic lithosphere, during the ascent of carbonatite magma through the lithospheric mantle. CO_2-rich fluid played a pivotal role in the formation of magnesite and this CO_2 is released from the carbonatite during its upwards migration. Our results demonstrate that CO_2 outflux through the mantle via plume-induced calcio-carbonatite can be entrapped in the peridotitic lithosphere by reacting with olivine and forming magnesite and siderite.

2. Geology of the area

The UACC of Sung Valley is hosted by the Shillong Plateau of NE India (Meghalaya) (Fig. 1a, b). This UACC is associated with the Kerguelen plume (Veena *et al.* 1998; Ray *et al.* 1999, 2000; Srivastava *et al.* 2005; Srivastava, 2020). The Shillong plateau is rectangular in shape and covers an area of about 4×10^4 km^2 (Srivastava & Sinha, 2004). This plateau appears as a block of uplifted Precambrian basement and shows a horst-like feature. The E–W-trending Brahmaputra and Dauki fault systems border the Shillong plateau in the north and south, respectively. The NW–SE-trending Kopali fracture zone and the N–S-trending Jamuna fault system characterize the east and west margins of this plateau (Evans, 1964; Desikachar, 1974; Nandy, 1980; Acharya *et al.* 1986; Gupta & Sen, 1988; Srivastava & Hall, 1995). The N–S-trending Um–Ngot lineament cuts across the Shillong plateau. This lineament contains several alkaline intrusive bodies including the Sung Valley UACC and it is related to the Ninety-East Ridge in the Indian Ocean (Gupta & Sen, 1988).

The Sung Valley UACC is an oval-shaped plutonic complex emplaced within the Proterozoic Shillong Group of rocks and consists of ultramafics (serpentinized peridotite, pyroxenite and melilitolite), alkaline rocks (ijolite and nepheline syenite) and carbonatites (Srivastava & Sinha, 2004; Srivastava *et al.* 2005). The core of this complex is occupied by serpentinized peridotite, and these peridotites are rimmed by pyroxenite. Peridotite and pyroxenite are the earliest rock units of the Sung Valley UACC; ijolite, younger than these ultramafics, forms a ring structure. These three rock units constitute the major part of the Sung Valley UACC. Among all rock units, pyroxenite is dominant and occurs in the marginal part of the complex, which is in direct contact with the quartzites of Shillong Group. The pyroxenite is mostly monomineralic, greenish-black to black in colour and composed dominantly of diopside. Melilitolite intrudes peridotite and pyroxenite as small dykes. Nepheline syenite also occurs as dykes and veins. Carbonatites occupy mainly the southern part of the complex as small stocks, lenses and dykes, and also as veins within the pyroxenite. Carbonatites are the youngest members of this complex (Srivastava & Sinha, 2004).

Petrological and geochemical studies carried out in the past suggest that the carbonatite of the Sung Valley UACC was formed by carbonate magma generated through low-degree partial melting of metasomatized mantle peridotite at ≥ 25 kbar pressure (Srivastava & Sinha, 2004; Melluso *et al.* 2010). Ray *et al.* (1999) and Srivastava *et al.* (2005) carried out carbon and oxygen isotopic analyses of the UACC carbonatites and inferred incorporation of inorganic carbon from the lithospheric mantle. They further suggested that this inorganic carbon was sourced from ancient subducted oceanic crust. The carbonatites are enriched with light rare earth elements (LREEs; Srivastava & Sinha, 2004; Sadik *et al.* 2014), comparable to other well-known carbonatites (Cullers & Graf, 1984; Woolley & Kemp, 1989; Woolley *et al.* 1991; Srivastava, 1997; Harmer, 1999). This carbonatite consists mainly of calcite and minor dolomite with accessory apatite and magnetite. Noble gas analysis of apatite from the carbonatites of Sung Valley indicates its crystallization during the waning stage of plume magmatism (Basu & Murty, 2006). It also shows significant contributions of mid-ocean-ridge basalt (MORB) and lithospheric components during crystallization of accessory apatite. Sr–Nd–Pb isotopic ratios of the Sung Valley carbonatite also indicate the interaction of plume with the continental lithosphere (Srivastava *et al.* 2005). The Sung Valley UACC has been dated by several different methods, giving a range of ages between 100 and 110 Ma (Ray & Pande, 2001; Srivastava & Sinha, 2004; Srivastava *et al.* 2019).

3. Analytical techniques

Petrographic and electron microprobe analyses were carried out on thin-sections. Mineral chemistry was obtained using a CAMECA SXFiveSA electron probe microanalyser (EPMA) at the Department of Geology, Institute of Science, Banaras Hindu University. Wavelength- dispersive spectrometry and a LaB6 source were used to carry out quantitative analyses. A voltage of 25 kV and beam current of 10 nA with a diameter of 1 μm were used. Thallium acid phthalate (TAP), large pentaerythritol (LPET) and large lithium fluoride (LLIF) crystals were used for measurements. Various natural and synthetic standards for rock-forming silicate minerals (diopside, peridote, almandine, albite and orthoclase) were used to calibrate the instrument. For major oxides, less than 1% precision was obtained. Raman spectroscopy was carried out using Horiba Jobin Yvan Lab Ram HR Laser Raman MicroProbe in Raman and Fluid Inclusion Laboratory at Wadia Institute of Himalayan Geology, Dehradun. This instrument includes an 800-nm focal length spectrometer, 514- and 780-nm argon ion lasers, detector charge-coupled device (CCD), edge filters and a trinocular Olympus microscope for both incident and transmitted light. The instrument has a spectral resolution of < 1 cm^{-1}. In the present study, a 514-nm laser of argon ion (Ar^+) source was used. For calibration, standard silicon was used, which shows Raman shift at 520.59 cm^{-1}. Calibration was performed with an error of 0.1 cm^{-1}. All the measurements were performed using a 100× objective. Repeated spectra were recorded in the 100–4000 cm^{-1} region to obtain a better signal-to-noise ratio. Isotopic ratios (for stable carbon and oxygen isotopes) of carbonatite samples from Sung Valley were obtained using gas-source continuous-flow isotope-ratio mass spectrometer (CF-IRMS) through GasBench at Wadia Institute of Himalayan Geology (WIHG), Dehradun. Small chips of fresh and unaltered calciocarbonatite samples (confirmed in thin-sections) were crushed and pulverized using an agate carbide ring grinder. This dry sample powder (100–200 μg) of pure calciocarbonatite was first put in 12 mL vials at 72°C in the GasBench tray and flushed with ultrapure He gas (≥ 99.9995%). In this way, all atmospheric gases from the vials were removed. Dry sample powder of calciocarbonatite was subjected to acidizing process with the injection of *c.* 50–70 μL phosphoric acid (≥ 99%). Thereafter, all the samples were kept at 72°C for 40–50 minutes to equilibrate and produce

https://doi.org/10.1017/S0016756820000631 Published online by Cambridge University Press

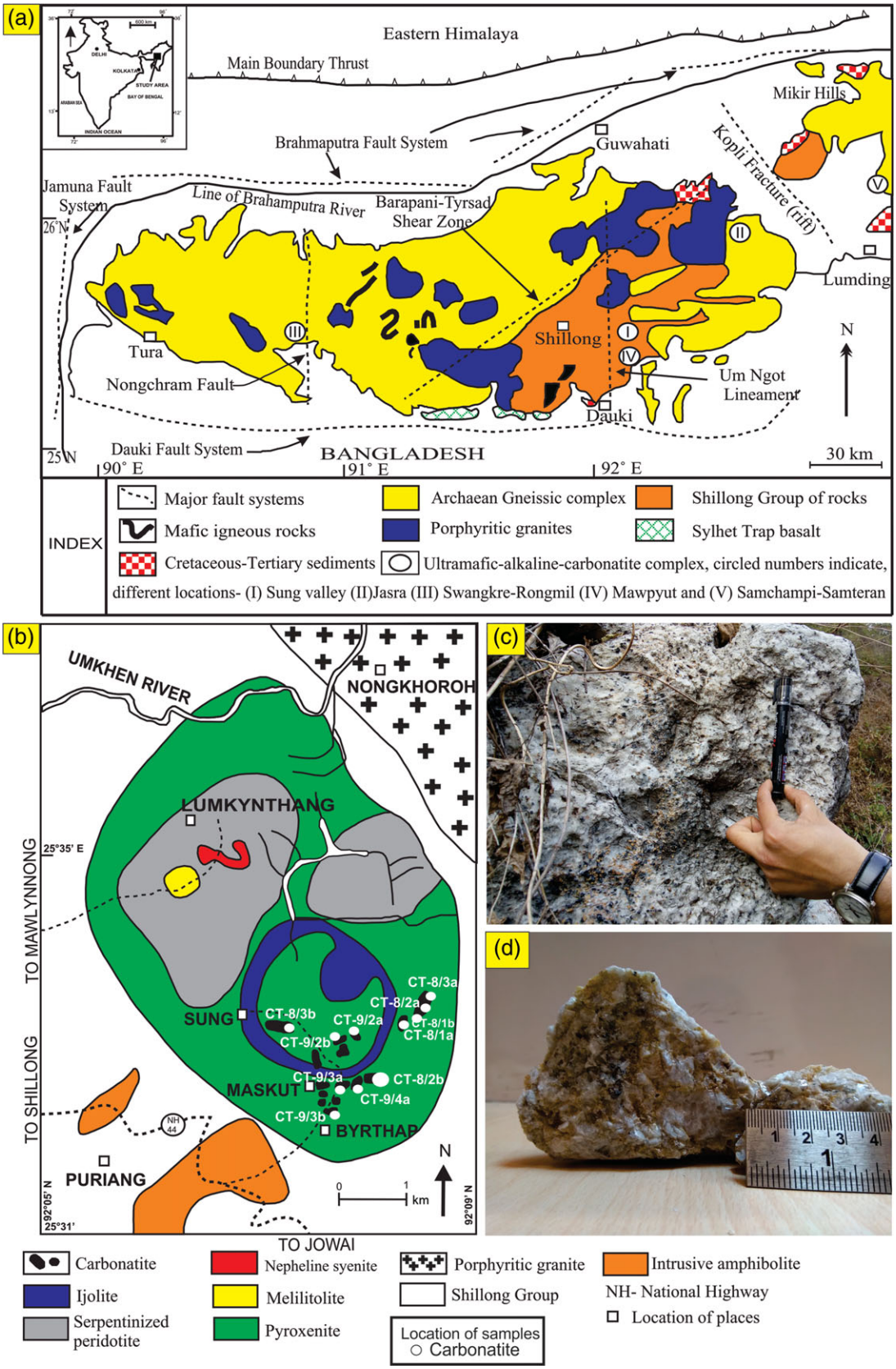

Fig. 1. (Colour online) (a) Geological map of Shillong plateau. (b) Geological map of Sung Valley, Meghalaya. (c) An outcrop of carbonatite from Sung Valley, Meghalaya. (d) Section of a hand specimen of carbonatite sample, no. CT-8/2b. (a, b) Modified after Srivastava & Sinha (2004).

https://doi.org/10.1017/S0016756820000631 Published online by Cambridge University Press

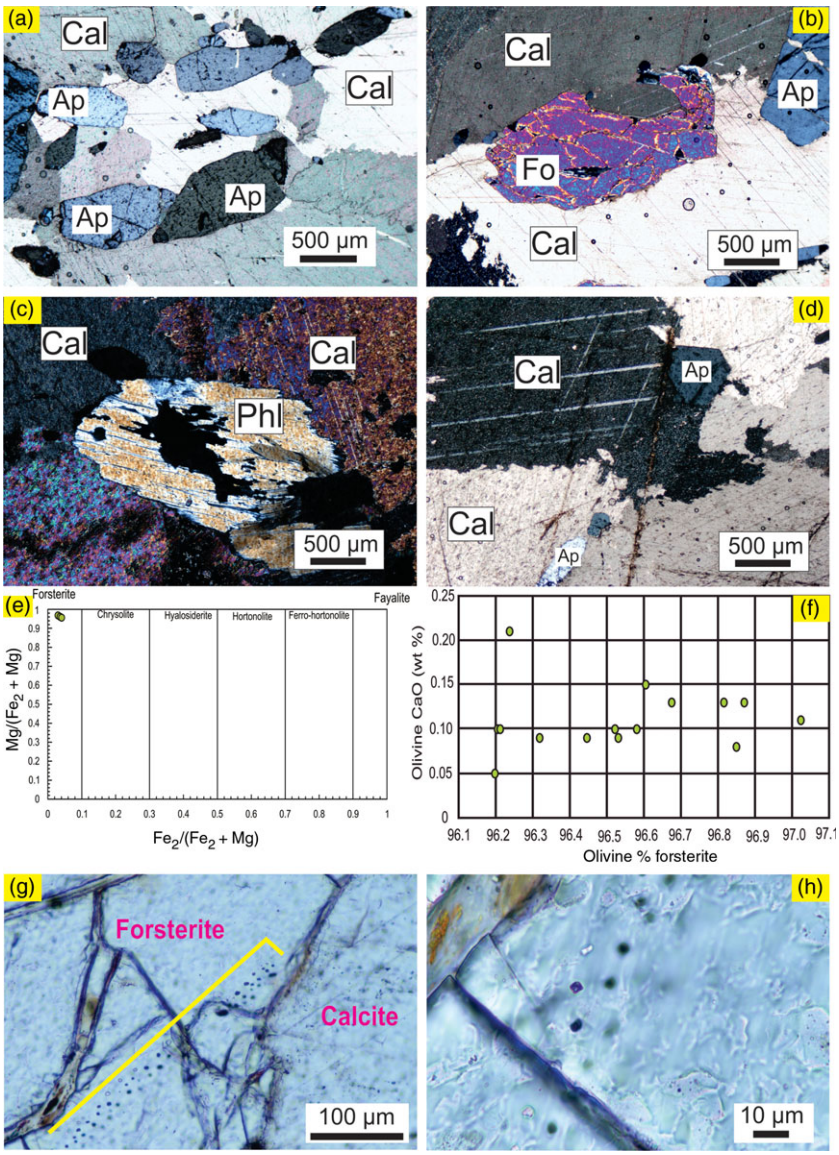

Fig. 2. (Colour online) (a) Cross-polarized photomicrograph showing coarse-grained calcite with subhedral to anhedral apatites in carbonatite sample (CT-8/2b). (b) Cross-polarized photomicrograph showing presence of forsterite xenocryst with resorbed boundary. (c, d) Petrographic features of analysed carbonatite samples, showing presence of phlogopite and calcite with euhedral to subhedral apatites, respectively. (e) Mg/(Fe_2 + Mg) v. Fe_2/(Fe_2 + Mg) plot representing the position of forsterite xenocryst on Fo–Fy series. The plot was constructed with the EPMA data and this xenocryst fell on the forsterite side on the Fo–Fy solid solution series. (f) Scatter plot of CaO content of xenocrystic olivine v. olivine % forsterite. The field of xenocryst compositions is referred from Spargo (2007). (g) Plane-polarized photomicrograph of a trail of solid inclusions restricted within forsterite xenocryst (shown with yellow line). (h) Plane-polarized photomicrograph of solid inclusions in forsterite, on higher magnification. Ap – apatite; Cal – calcite; Fo – forsterite; Phl – phlogopite.

carbon dioxide. CO_2 formed by this process was introduced into the IRMS through the gas chromatography (GC) column to analyse the isotopic ratio of carbon and oxygen. The $\delta^{13}C$ and $\delta^{18}O$ in the present study are reported with respect to V-PDB (Pee Dee Belemnite) and V-SMOW (Vienna Standard Mean Ocean Water) standards, respectively, using:

$$\delta = \left[\left(R_{\text{sample}}/R_{\text{standard}}\right) - 1\right] \times 10^{-3},$$

where R is either $^{13}C/^{12}C$ or $^{18}O/^{16}O$.

Final isotopic ratios of $\delta^{13}C$ and $\delta^{18}O$ were obtained using the Santrock, Studley and Hayes (SSH) correction (Santrock *et al.* 1985). Precision better than ± 0.1‰ for $\delta^{13}C$ and $\delta^{18}O$ was achieved. For calibration, primary standard NBS-18 was used, whereas in-house standard Merck-$CaCO_3$ at the interval of 10 samples was used to verify the precision and quality of the measurement. Inductively coupled plasma – mass spectrometer (ICP-MS; Perkin-Elmer SCIEX ELAN DRC-e) at the WIHG was used to determine REE concentration. An open-system digestion method was chosen for sample preparation. Powder (0.1 g) from each carbonatite sample was separately mixed with an HF and HNO_3 (2:1 ratio) solution in Teflon crucibles. Crucibles were then heated over a hot plate until the powdered samples were completely digested. Accuracy range for REE analysis was 2–12%, and precision varied over the range 1–8%. Rock standards (JG-2 and MB-H) were used to calibrate the ICP-MS instrument.

4. Results

A total of 11 fresh samples of carbonatites were collected from different locations (Fig. 1b). Almost all of the carbonatite sample locations are confined to the SE part of the complex. All of these samples represent fresh calcio-carbonatites, which belong to the sovitic carbonatites group (a coarse-grained variety). Two out of these 11 samples contain forsterite grains. However, only one or two forsterite grains were observed in petrographic thin-sections of these two samples.

4.a. Petrography

Our petrographic studies reveal that the Sung Valley carbonatite is coarse-grained and shows a hypidiomorphic texture. It is dominantly composed of calcite (80–90%) (Fig. 2a–d). Accessory

https://doi.org/10.1017/S0016756820000631 Published online by Cambridge University Press

Table 1. Composition of forsterite based on EPMA point analysis

Spot analysis	1 (core)	2 (rim)	3 (rim)	4 (rim)	5 (rim)	6 (core)	7 (core)	8 (rim)	9 (rim)	10 (core)	11 (core)	12 (rim)	13 (rim)	14 (core)	15 (core)
SiO_2	42.13	42.54	41.92	42.38	42.55	41.76	42.58	41.6	41.92	40.91	40.95	41.84	42.1	40.63	41.23
TiO_2	0	0	0	0.06	0.07	0.01	0	0	0.07	0.07	0.01	0	0.04	0.02	0.07
Al_2O_3	0	0	0.02	0.03	0.02	0.01	0.03	0.02	0.01	0.02	0.01	0	0.01	0.03	0.01
Cr_2O_3	0	0.02	0	0.02	0.02	0	0.01	0.02	0.02	0.01	0	0.02	0	0.04	0.02
FeO	3.87	3.71	3.3	3.72	3.49	3.47	3.78	3.04	3.27	3.86	3.46	3.56	3.19	3.35	3.16
MnO	0.37	0.29	0.47	0.24	0.23	0.36	0.34	0.43	0.31	0.28	0.38	0.41	0.22	0.38	0.29
MgO	54.72	54.3	54.08	53.32	54.51	53.94	54.21	55.51	55.54	54.88	54.55	54.51	55.13	53.38	54.87
CaO	0.05	0.09	0.13	0.21	0.1	0.09	0.1	0.11	0.13	0.1	0.1	0.09	0.08	0.15	0.13
Na_2O	0.01	0.01	0.01	0	0	0	0.03	0	0	0.02	0.01	0.01	0.02	0.02	0.02
K_2O	0	0.01	0	0.02	0.02	0.02	0	0.02	0.01	0.04	0.02	0.02	0.04	0.04	0.05
Total	101.37	100.97	100.13	99.99	101	99.87	101.07	100.92	101.47	100.43	99.7	100.66	101.02	98.24	100.04
On the basis of 4O															
Si	0.993	1.004	0.998	1.009	1.003	0.997	1.004	0.983	0.986	0.976	0.982	0.992	0.993	0.988	0.984
Ti	0	0	0	0.001	0.001	0	0	0	0.001	0.001	0	0	0.001	0	0.001
Al	0	0	0.001	0.001	0	0	0.001	0	0	0.001	0	0	0	0.001	0
Cr	0	0	0	0	0	0	0	0	0	0	0	0	0	0.001	0
Fe_3	0.004	0	0.003	0	0	0.004	0	0.003	0.003	0.004	0.004	0.004	0.003	0.004	0.003
Fe_2	0.076	0.073	0.066	0.074	0.069	0.069	0.075	0.06	0.064	0.077	0.069	0.071	0.063	0.068	0.063
Mn	0.007	0.006	0.01	0.005	0.005	0.007	0.007	0.009	0.006	0.006	0.008	0.008	0.004	0.008	0.006
Mg	1.923	1.91	1.919	1.893	1.915	1.92	1.905	1.956	1.946	1.952	1.949	1.927	1.937	1.935	1.951
Ca	0.001	0.002	0.003	0.005	0.003	0.002	0.003	0.003	0.003	0.003	0.003	0.002	0.002	0.004	0.003
Na	0	0.001	0	0	0	0	0.001	0	0	0.001	0.001	0	0.001	0.001	0.001
K	0	0	0	0.001	0.001	0.001	0	0.001	0	0.001	0.001	0.001	0.001	0.001	0.001
Total	3.005	2.996	3	2.989	2.996	3.001	2.996	3.015	3.011	3.021	3.017	3.006	3.006	3.01	3.014
Mg no.[a]	96	96	97	96	96	96	96	97	96	96	96	96	97	97	97

[a]Mg no. = 100×Mg/(Mg+$Fe2^+$).

phases are mostly apatite, which is euhedral to subhedral in nature (Fig. 2a, d), along with phlogopite and magnetite (Fig. 2c). The carbonatite sample CT-8/2b containing one olivine xenocryst was collected from the SE part of the UACC (Fig. 1b, c). This sample consists of 80–90% calcite and *c.* 5% dolomite (Fig. 2a). The olivine xenocryst is *c.* 1.5 mm in size and shows resorbed texture (Fig. 2b; rim on the boundary), which confirms its early crystallization and reaction with carbonatitic melt.

4.b. Electron microprobe analysis

Electron microprobe analysis (EPMA) was carried out on 15 spots within one olivine xenocryst present in primary calciocarbonatite (Table 1). The olivine xenocryst is almost pure forsterite with 53.32–55.54% MgO, 3.04–3.87% FeO and 40.63–42.58% SiO_2, and a Mg number (100×(Mg/Fe^2 + Mg)) value of 96–97%. This indicates a forsterite end-member (Fig. 2e). This olivine is a xenocryst and not an accessory phase of carbonatite. This is confirmed by the presence of pure forsterite with very low CaO content (Fig. 2f and Table 1), which is not likely to form in a Ca-rich rock (Melluso *et al.* 2010). A plot of CaO < 0.2 (wt%) and % forsterite > 80 of forsterite xenocryst clearly confirms the disequilibrium between the forsterite xenocryst and carbonatite melt at the time of incorporation of xenocryst in the melt (Fig. 2f).

4.c. Inclusion petrography

Solid inclusions were observed in the forsterite xenocryst and fluid inclusions in apatite. The forsterite xenocryst hosts a pseudosecondary, intragranular solid inclusion trail, which is confined within this crystal boundary (Fig. 2g) (Roedder, 1984). These inclusions are solid mineral phases as indicated by their saccharoidal appearance (Figs 2h, 3a, d (inset), e (inset)). They range in size from 2 to 4 μm and are formed as a result of fracture healing during the growth of forsterite crystal (Roedder, 1984). Accessory apatite hosts discrete primary fluid inclusions of various shapes including elliptical to tabular, which are 20–40 μm in size (Fig. 4a (inset), c (inset)). Among them, polyphase and biphase (liquid + vapour) fluid inclusions were considered because they occur in the core of apatite crystals. The occurrence of these fluid inclusions in such a microstructural position suggests primary trapping during growth of its host crystal (Roedder, 1984).

https://doi.org/10.1017/S0016756820000631 Published online by Cambridge University Press

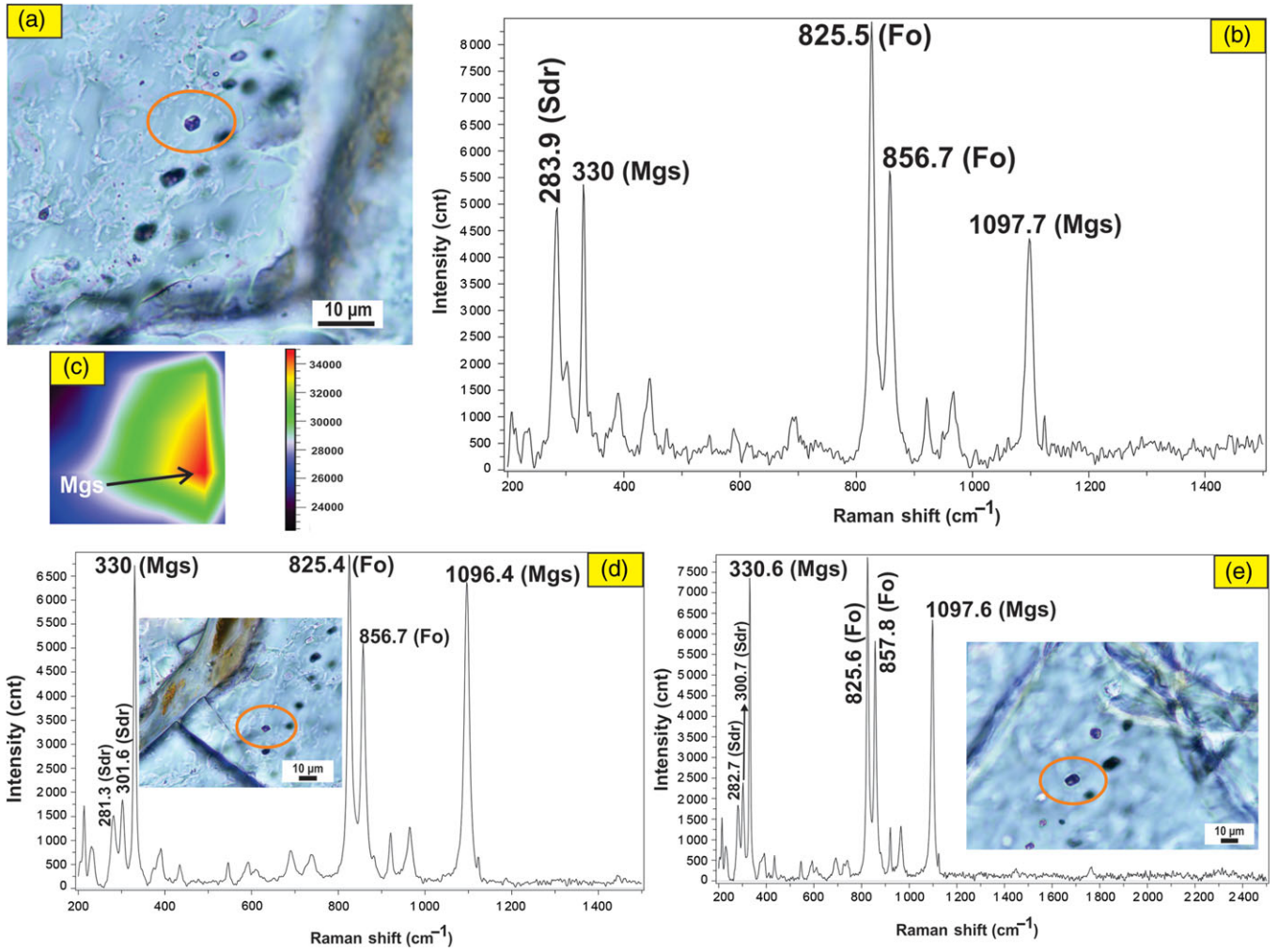

Fig. 3. (Colour online) (a) Plane-polarized photomicrograph of saccharoidal solid inclusions in forsterite on higher magnification. (b) Raman spectrum of forsterite (Fo) host, along with magnesite (Mgs) and siderite (Sdr). (c) Mapping in the *x*–*y* plane of the solid inclusions, indicating the presence of magnesite. Red–green–blue colours in the map are assigned to intensity of major peak 1097.7 cm^{-1}. (d, e) Additional Raman spectra of solid inclusions (another spots). Insets show high-resolution plane-polarized photomicrographs of the inclusions.

4.d. Raman spectroscopy of inclusions

The phase composition of the forsterite-hosted saccharoidal solid inclusion trail was investigated by Raman microspectroscopy. The Raman spectrum shows the host as forsterite with Raman shifts at 825.5 and 856.7 cm^{-1} (Fig. 3b). Crystalline phases of these inclusions were identified as magnesite. It shows characteristic Raman shifts at 1097.7 cm^{-1}, which is symmetric stretching vibration v_1, and 330 cm^{-1}, which is strong vibration *s* (Fig. 3b) (Frezzotti *et al.* 2012). Siderite is also detected with Raman shift at 283.9 cm^{-1}, which is translational lattice mode with a shoulder peak at around 300 cm^{-1} (Fig. 3b) (Frezzotti *et al.* 2012). Usually, translational lattice modes in magnesite and siderite show slightly less intensity than the symmetric stretching vibration v_1. However, in some cases and in the present study, *T* vibrations (translational lattice modes) show slightly higher intensity than the v_1 bands (i.e. RRUFF ID X050115 and X050116 for magnesite and X050143 for siderite). In these Raman spectra (Fig. 3), all the vibrations of carbonates (magnesite and siderite) result in narrow FWHM (full width of the Raman peak at half maximum height), which further confirm the high crystallinity of these inclusions. Due to the occurrence of these two carbonates together and absence of v_1 vibrations of siderite at *c.* 1090 cm^{-1}, we have used the term Fe-rich magnesite or (Fe, Mg)CO_3. Raman mapping of these saccharoidal inclusions in the *x*–*y* plane confirms the presence of magnesite (Fig. 3c). Raman microspectroscopy spot analysis of representative polyphase primary fluid inclusions hosted by apatite (Fig. 4a (inset)) was also carried out. The liquid and vapour phases were identified as water and CO_2 (Fig. 4b). Host apatite shows Raman shift at 967.2 cm^{-1} and asymmetric hump (fitted with standard spectrum) at around 3000–4000 cm^{-1}, indicating the presence of water with CO_2 (Fig. 4b). Additional Raman spectra of solid inclusions within the forsterite xenocryst are shown in Figure 3d and e, while the additional spectrum for biphase fluid inclusions in apatite is provided in Figure 4c.

4.e. Stable isotope and bulk-rock geochemistry

Eight representative samples of carbonatite were analysed for stable isotopes of ^{18}O and ^{13}C. Oxygen isotope data of our samples fall in the range of +7.88‰ to +9.22‰ with ±0.1‰ precision (Fig. 5; Table 2). This suggests that the carbonatite is primary and of mantle origin (Taylor *et al.* 1967; Deines & Gold, 1973; Sheppard & Dawon, 1973). Carbon isotope values, on the other hand, fall in

https://doi.org/10.1017/S0016756820000631 Published online by Cambridge University Press

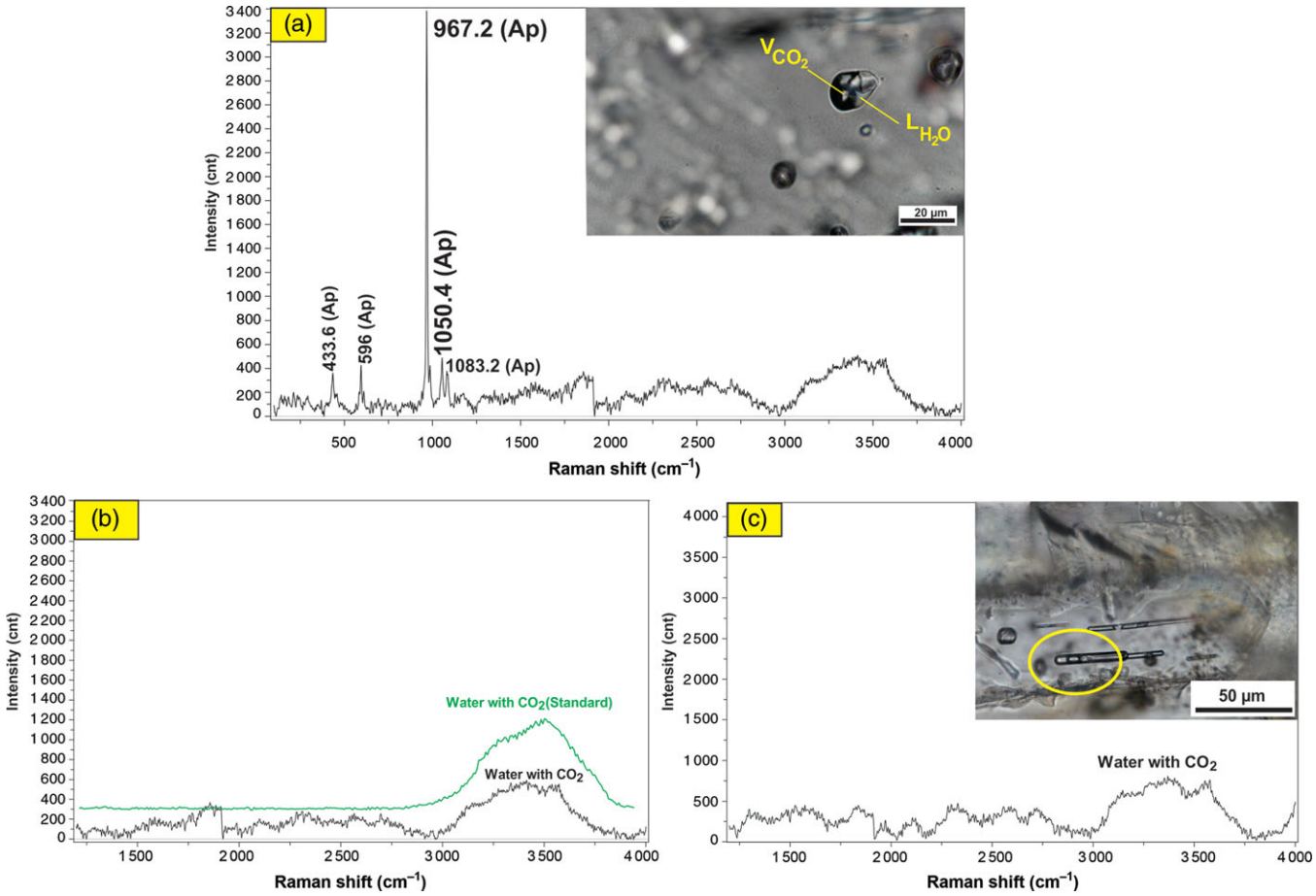

Fig. 4. (Colour online) (a) Raman spectrum of host apatite. Inset shows plane-polarized photomicrograph of elliptical polyphase primary fluid inclusions in apatite, showing vapour phase of CO_2 and liquid H_2O. (b) Extracted Raman spectrum of (a) fitted with standard spectrum, showing presence of water with CO_2. Spectrum standard used for reference: quality of spectrum, water with CO_2; library, minlabv5.lib (spectrum id: NGS26E9.spc). (c) Raman spectrum of tabular biphase fluid inclusion in apatite showing the presence of water with CO_2. Inset shows the photomicrograph of analysed fluid inclusion. Ap – apatite.

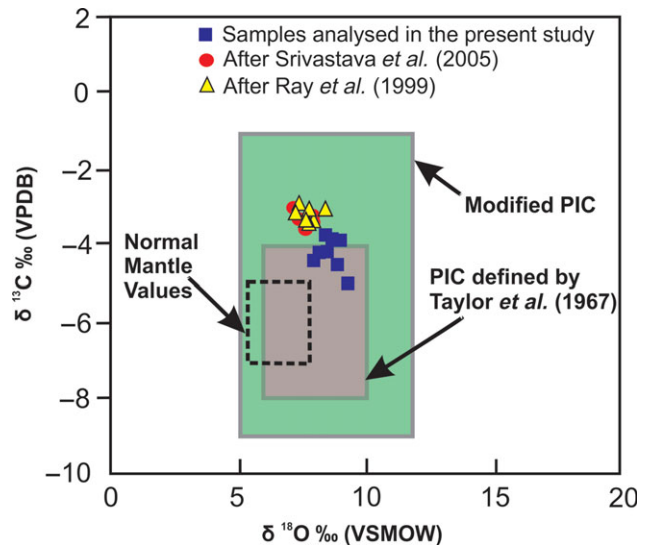

Fig. 5. (Colour online) Carbon and oxygen ($\delta^{13}C$ and $\delta^{18}O$) isotopic compositions of Sung Valley carbonatites. Primary igneous carbonatites (PIC) defined after Taylor *et al.* (1967), modified PIC after Deines (1989) and Keller & Hoefs (1995), and normal mantle values after Kyser (1990) and Keller & Hoefs (1995).

the range of −3.70‰ to −4.96‰ with ±0.1‰ precision and indicate some enrichment compared with normal mantle values ($\delta^{13}C = -5‰$ to −8‰) (Fig. 5; Table 2). Stable isotopic (C and O) data in this study corroborate previously obtained data (Srivastava *et al.* 2005).

These same eight samples were chosen for whole-rock geochemistry (Table 3) and were analysed for REE content; total abundance ranged widely from 737 to 1219 ppm (Table 3). A chondrite-normalized REE plot (Boynton, 1984) shows enrichment of LREEs compared with heavy REEs (HREEs) (Fig. 6).

5. Discussion

5.a. Interaction of carbonatitic magma with the peridotitic lithosphere

Petrographic and EPMA analyses of sample CT-8/2b provide direct evidence of the interaction between carbonatitic melt and the peridotitic lithosphere. The xenocrystic nature of the olivine crystal is confirmed by its pure forsteritic nature with very low CaO content (Fig. 2f; Table 1), which is not likely to form in a Ca-rich rock. Olivine present in the Sung Valley carbonatite was earlier interpreted as a conspicuous silicate phase (e.g. Melluso

https://doi.org/10.1017/S0016756820000631 Published online by Cambridge University Press

Table 2. Isotopic data obtained for stable isotopes of carbon and oxygen, from the analysis of carbonatites of Sung Valley, Meghalaya. The standard deviation for $\delta^{13}C$ and $\delta^{18}O$ is ±0.1‰

Sample ID	$\delta^{13}C$ ‰ (VPDB)	$\delta^{18}O$ ‰ (VSMOW)
CT-8/1a	−3.82	8.89
CT-8/1b	−4.46	8.80
CT-8/2b	−4.35	7.88
CT-8/2a	−4.96	9.22
CT-8/3a	−4.12	8.40
CT-8/3b	−4.15	8.05
CT-9/2b	−3.79	8.57
CT-9/3b	−3.70	8.32

et al. 2010; Sai & Sengupta, 2017). These workers suggested that this olivine is in equilibrium with the carbonatite melt. However, a plot between CaO (wt%) and % forsterite (Fig. 2f) suggests that this olivine was not in equilibrium. It shows minimum % forsterite values of *c.* 96. For this olivine to be in equilibrium, the points should fall at *c.* 80 (Spargo, 2007; Brenna *et al.* 2018). It may also be noted that these olivine grains are too rare in Sung Valley carbonatite to be considered an accessory phase. We have carried out petrographic analysis of 11 samples of carbonatites, and olivine was observed in only 2 of them. This paucity also suggests the xenocrystic nature of olivine in Sung Valley carbonatite. We therefore inferred that the olivine xenocryst was scavenged from the peridotitic lithosphere by carbonatite melt.

Experiments suggest that due to the very fast penetrative infiltration mechanism of carbonatite magma in polycrystalline olivine (in peridotites) (Hammouda & Laporte, 2000), chemical exchange between carbonatite melt and rock matrix took place (Green & Wallace, 1988; Yaxley *et al.* 1991; Hauri *et al.* 1993; Rudnick *et al.* 1993) and carbonatite melt metasomatizes the mantle rocks at the time of ultrafast mantle impregnation. As a consequence, with the dissolution of olivine from peridotite, forsterite is reprecipitated in carbonatite reservoir (Hammouda & Laporte, 2000).

It can therefore be argued that the forsterite xenocryst investigated was originally from the peridotitic lithosphere that became engulfed in ascending carbonatitic magma and was subsequently altered by dissolution precipitation process. This occurred during upwards migration of carbonatitic magma through the peridotitic lithosphere, and the forsterite must have precipitated initially in euhedral form. However, its boundaries became resorbed and gave it a subhedral to anhedral shape during its interaction with the carbonatitic magma. Complete resorption could not take place, as the xenocryst was not in equilibrium with the carbonatite magma (Fig. 2f).

Our geochemical analyses show enrichment of REEs, specifically LREEs with a high La/Yb ratio (Table 3; Fig. 6), in carbonatite, which is similar to the results obtained by earlier workers researching the Sung Valley UACC (Srivastava *et al.* 2005; Sadik *et al.* 2014). Carbonatitic melts generated from partial melting of carbonated peridotites are extremely enriched in incompatible elements, especially LREEs, and are highly metasomatic in nature (Green & Wallace, 1988; Ionov *et al.* 1993; Rudnick *et al.* 1993; Yaxley *et al.* 1998; Blundy & Dalton, 2000; Hammouda & Laporte, 2000; Grassi & Schmidt, 2011; O'Reilly & Griffin, 2013; Sokol *et al.* 2016; Gervasoni *et al.* 2017). The metasomatic nature of this carbonatite is evident from our EPMA analysis that reveals the highly forsteritic nature of the olivine xenocryst (% forsterite *c.* 97; Fig. 2e). This is a typical evidence of carbonate metasomatism of the mantle peridotites caused by the migration of carbonatitic magma through peridotitic lithosphere (Hammouda & Laporte, 2000; Su *et al.* 2016).

As described by Srivastava *et al.* (2005), the interaction of carbonatitic melt with the lithosphere is also well established by isotopic studies in the Sung Valley UACC. This in turn indicates that the carbonation of the lithospheric mantle took place during ascent of carbonatitic magma through the mantle lithosphere. Our results, integrated with existing isotopic data, therefore clearly suggest that carbonatitic magma interacted with and metasomatized the lithospheric mantle in the Sung Valley UACC during its ascent.

5.b. Formation of magnesite due to carbonation of forsterite by primary igneous carbonatite magma

The occurrence of Fe-rich magnesite inclusion trail only in forsterite crystal implies that forsterite was subjected to carbonation in the presence of CO_2 at the time of its precipitation and crystallization. As a result, Fe-rich magnesite was formed (Xiong & Giammar, 2014; Loring *et al.* 2015; Stopic *et al.* 2018). Since this forsterite is a xenocryst, we envisage that this trail of inclusions has formed as a result of healing fractures during forsterite crystal growth. There is another possibility of magnesite being a secondary inclusion entrapped after the formation of forsterite. Both these processes can occur during carbonation of forsterite while within the carbonatitic magma at the time of its growth or after the completion of crystallization. This trail could therefore be pseudosecondary or secondary in nature (Roedder, 1984). Abovementioned carbonation reaction can be described by the relevant $MgO–CO_2$ system (Stopic *et al.* 2018).

The formation of magnesite through carbonation takes place through the following exothermic reaction:

$$MgO_{(s)} + CO_{2(g)} = MgCO_{3(s)} + \text{energy},$$

where the subscripts s and g refer to the state (solid and gas, respectively).

The carbonatites from Sung Valley UACC are characterized by primary fluid inclusions of water with CO_2 (Fig. 4) in accessory apatite, which are the essential fluid components of carbonatitic magma (Ray & Ramesh, 2006). Carbonatite is characterized by its CO_2-rich composition (Bailey & Hampton, 1990; Dawson *et al.* 1994; Dixon *et al.* 1997; Lee & Wyllie, 1998; Ray & Ramesh, 2006; Jones *et al.* 2013) and considered as a major carrier of CO_2 and H_2O fluids in the mantle (Ray & Ramesh, 2006). After combining experimental studies on mantle-related carbonatites, Harmer (1999) showed that low-viscosity carbonatitic melt can percolate upwards and generate free fluid (CO_2) and metasomatic olivine. We therefore suggest that these fluid phases (H_2O and CO_2) from ascending carbonatite in accessory apatite formed magnesite by interacting with olivine from the lithospheric mantle.

We carried out stable isotope analysis to confirm that the magnesite is not a product of alteration or hydrothermal reactions in the carbonatite. Our C and O isotopic analyses reaffirm the fact that these carbonatites were not affected by any secondary hydrothermal alteration, shallow crustal contamination or even magmatic fractionation (Fig. 5). Moreover, the effect of fractional crystallization can also be ruled out, as in such cases $\delta^{18}O$ and $\delta^{13}C$ values are scattered (Deines, 1989; Ray & Ramesh, 2000),

https://doi.org/10.1017/S0016756820000631 Published online by Cambridge University Press

Table 3. Rare earth element concentration (ppm) of Sung Valley carbonatites, analysed by ICP-MS

Sample no.	La	Ce	Pr	Nd	Sm	Eu	Gd	Tb	Dy	Ho	Er	Tm	Yb	Lu	∑REE
CT-8/2a	211.48	458.25	58.14	218.73	35.77	9.779	31.79	3.468	14.52	2.27	5.01	0.54	2.98	0.41	1053.18
CT-8/1a	228.75	520.67	69.44	272.61	44.58	11.96	38.13	4.172	16.85	2.55	5.46	0.54	3.00	0.42	1219.18
CT-8/2b	201.91	436.86	55.84	211.40	34.82	9.517	30.56	3.399	14.05	2.16	4.85	0.51	2.81	0.39	1009.12
CT-8/1b	203.20	438.20	55.71	210.53	34.63	9.469	30.85	3.396	13.97	2.19	4.84	0.51	2.83	0.40	1010.79
CT-8/3b	182.00	393.16	50.03	190.40	30.68	8.463	27.20	3.025	12.52	1.96	4.33	0.45	2.50	0.34	907.12
CT-8/3a	182.31	395.83	50.51	192.61	31.47	8.624	28.08	3.048	12.66	1.95	4.41	0.45	2.54	0.35	914.904
CT-9/2b	209.56	476.15	62.58	244.26	41.09	11.00	35.99	3.917	16.15	2.45	5.33	0.55	3.01	0.42	1112.50
CT-9/3b	136.15	310.31	41.85	166.79	27.89	7.575	24.57	2.675	11.05	1.69	3.75	0.37	2.08	0.28	737.09

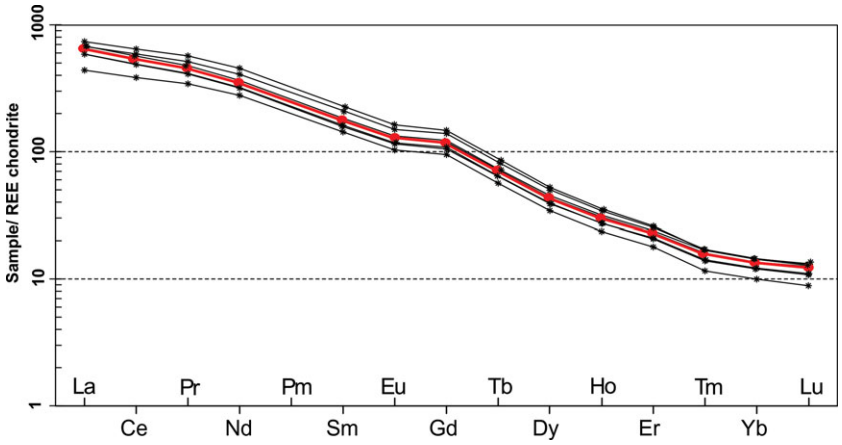

Fig. 6. (Colour online) Chondrite-normalized rare earth element patterns for carbonatite samples of Sung Valley. (Analysed sample no. CT-8/2b is highlighted in red with unique symbols.) Chondrite values after Boynton (1984).

unlike the clustered narrow range of values obtained here (Fig. 5). The $\delta^{18}O$ values are restricted between 1‰ and 10‰ (mantle values; Fig. 5) and rule out any possibility of fluid loss during the emplacement of these carbonatites (Ray *et al.* 1999). All the samples we analysed fall within the primary igneous carbonatites field. This field represents the primary isotopic composition of typical igneous carbonatites of mantle origin (Keller & Hoefs, 1995). Here 'primary' indicates carbonatites that are unaffected by surficial secondary processes. Our $\delta^{13}C$ and $\delta^{18}O$ values tend towards the primary igneous carbonatite values defined by Taylor *et al.* (1967), which are much closer to normal mantle values, negating the possibility of any secondary alteration processes. It is worth noting that $^{87}Sr/^{86}Sr$ and $^{143}Nd/^{144}Nd$ isotopic ratios of Sung Valley carbonatites obtained by Veena *et al.* (1998) and Ray *et al.* (2000) also indicate that these carbonatites are unaffected by crustal contamination. Sr^{86}/Sr^{87} and $\delta^{18}O$ isotopic study by Srivastava *et al.* (2005) also indicate that the Sung Valley carbonatite is not affected by any crustal contamination and hydrothermal alteration. Our inference is in accordance with that of Srivastava *et al.* (2005), who suggested derivation of this carbonatite from low-degree (*c.* 0.1%) partial melting of carbonated mantle peridotite. Our stable isotope analysis indicates two things. First, no enrichment of ^{18}O indicates that the carbonatites were not affected by any magmatic fractionation or secondary hydrothermal processes (Table 2). Second, $\delta^{13}C$ values (−3.70‰ to −4.96‰) indicate the incorporation of recycled inorganic carbon (Table 2). Our isotopic results are comparable with previous work where it is suggested that this inorganic carbon was originally derived from ancient subducted oceanic crusts (Ray *et al.* 1999). Our stable isotope analysis therefore negates the possibility of magnesite formation through any hydrothermal or crustal contamination process, and reaffirms its formation through metasomatism of forsterite by CO_2-rich fluids originated from carbonatite magma.

5.c. Implications for CO_2 entrapment in the lithospheric mantle

The crux of the present study is the formation of (Fe, Mg)CO_3 in olivine from peridotitic lithosphere by CO_2- and H_2O-bearing carbonate-rich fluids. Formation of Fe-rich magnesite in olivine by CO_2 is a very important global phenomenon that helps sequestration of atmospheric CO_2 in geological reservoirs (Kelemen & Matter, 2008). Metasomatism of peridotitic rocks by CO_2-rich fluid can efficiently form magnesite in peridotitic rocks by post-entrapment carbonation reaction (Berkesi *et al.* 2012). Experimental studies have shown that CO_2-saturated aqueous fluid and H_2O-saturated supercritical CO_2 can readily form magnesite by reacting with olivine/forsterite (Kwak *et al.* 2011; Todd Schaef *et al.* 2013; Loring *et al.* 2015; Stopic *et al.* 2018). Precipitation of Mg- and Fe-carbonates during these reactions is further facilitated by fractures present in the rocks (Xiong & Giammar, 2014). Carbonatitic magma not only has the lowest viscosity among all types of magmas, but also has low interfacial energy with respect to mantle minerals (Dobson *et al.* 1996). This enables migration of carbonate-rich melt through grain boundary networks even with very low porosities, and can cause

https://doi.org/10.1017/S0016756820000631 Published online by Cambridge University Press

widespread metasomatism of the upper mantle. In the present study, we have shown that one important aspect of carbonation or CO_2 outgassing of the upper mantle due to metasomatism by carbonatitic melt is the formation of magnesite. It is envisaged that CO_2 derived from the metasomatic carbonatitic fluid becomes entrapped within the lithospheric mantle by reacting with peridotite. This reaction forms magnesite or Fe-rich magnesite.

6. Conclusions

The presence of forsterite xenocryst within carbonatite of Sung Valley UACC suggests the interaction of peridotitic lithosphere with plume-derived carbonatitic magma.

Petrographic and mineral chemistry data suggest the dissolution of olivine from lithospheric peridotite by carbonatitic magma and reprecipitation of forsterite.

CO_2 and H_2O from the carbonatitic magma penetrated the forsterite xenocryst and formed magnesite and siderite when the forsterite was in the carbonatite magma.

We suggest that, by formation of carbonates in the peridotitic lithosphere during carbonate magmatism, a considerable amount of mantle-derived CO_2 can become entrapped within the lithosphere.

Acknowledgement. The Director of WIHG is thanked for encouragement and support. Drs Rajesh Sharma (WIHG) and Bhanu Pratap (NPL) are thanked for help and suggestions regarding Raman spectroscopy. We thank NV Chalapathi Rao and Dinesh Pandit, Department of Geology, Banaras Hindu University (BHU) for carrying out the electron probe microanalyses under the DST-FIST and DST-PURSE sponsored programme. Sakshi Maurya is thanked for stable isotope analysis. AK Singh is thanked for help and suggestions regarding ICP-MS analysis. The authors take full responsibility for all the data and their interpretations. We thank the editor, Kathryn Goodenough, and two anonymous reviewers for thorough and constructive reviews. This work is part of the doctoral thesis of SC on the Sung Valley UACC, Meghalaya, India.

References

Acharya SK, Mitra ND and Nandy DR (1986) Regional geology and tectonic setting of Northeast India and adjoining region, in geology of Nagaland Ophiolite. *Memoirs of the Geological Survey of India* **119**, 6–12.

Bailey DK and Hampton CM (1990) Volatiles in alkaline magmatism. *Lithos* **26**, 157–65.

Basu S and Murty SVS (2006) Noble gases in carbonatites of Sung Valley and Ambadongar: implications for trapped components. *Chemical Geology* **234**, 236–50, https://doi.org/10.1016/j.chemgeo.2006.05.004.

Berkesi M, Guzmics T, Szabó C, Dubessy J, Bodnar RJ, Hidas K and Ratter K (2012) The role of CO_2-rich fluids in trace element transport and metasomatism in the lithospheric mantle beneath the Central Pannonian Basin, Hungary, based on fluid inclusions in mantle xenoliths. *Earth and Planetary Science Letters* **331**, 8–20, https://doi.org/10.1016/j.epsl.2012.03.012.

Blundy J and Dalton J (2000) Experimental comparison of trace element partitioning between clinopyroxene and melt in carbonate and silicate systems, and implications for mantle metasomatism. *Contributions to Mineralogy and Petrology* **139**, 356–71.

Boyd FR, Pokhilenko NP, Pearson DG, Mertzman SA, Sobolev NV and Finger LW (1997) Composition of the Siberian Cratonic Mantle: evidence from Udachnaya peridotite xenoliths. *Contributions to Mineralogy and Petrology* **128**, 228–46, https://doi.org/10.1007/s004100050.

Boynton WV (1984) Cosmochemistry of the rare earth elements: meteorite studies. In *Rare Earth Element Geochemistry* (ed. P Henderson), pp. 63–114. Amsterdam: Elsevier, Developments in Geochemistry no. 2.

Brenna M, Cronin SJ, Smith IE, Tollan PM, Scott JM, Prior DJ, Bambery K and Ukstins IA (2018) Olivine xenocryst diffusion reveals rapid monogenetic basaltic magma ascent following complex storage at Pupuke Maar, Auckland Volcanic Field, New Zealand. *Earth and Planetary Science Letters* **499**, 13–22, https://doi.org/101016/jepsl201807015.

Cullers RL and Graf JL (1984) Rare earth elements in igneous rocks of the continental crust: predominantly basic and ultrabasic rocks. In *Rare Earth Element Geochemistry* (ed. P Henderson), pp. 237–74. Amsterdam: Elsevier, Developments in Geochemistry no. **2**

Dalton JA and Wood BJ (1993) The compositions of primary carbonate melts and their evolution through wallrock reaction in the mantle. *Earth and Planetary Science Letters* **119**, 511–25.

Dawson JB, Pinkerton H, Pyle DM and Nyamweru C (1994) June 1993 eruption of Oldoinyo Lengai, Tanzania: exceptionally viscous and large carbonatite lava flows and evidence for coexisting silicate and carbonate magmas. *Geology* **22**, 799–802.

Deines P (1989) Stable isotope variations in carbonatites. In *Carbonatites: Genesis and Evolution* (ed. K Bell), pp. 301–50. Boston: Unwin Hyman.

Deines P and Gold DP (1973) The isotope composition of carbonatites and kimberlite carbonate and their bearing on the isotopic composition of deep seated carbon. *Geochimica et Cosmochimica Acta* **37**, 1709–33.

Desikachar SV (1974) A review of the tectonic and geologic history of Eastern India in terms of plate tectonics theory. *Journal of Geological Society of India* **15**, 137–49.

Dixon J, Clague DA, Cousens B, Monsalve ML and Uhl J (2008) Carbonatite and silicate melt metasomatism of the mantle surrounding the Hawaiian plume: evidence from volatiles, trace elements, and radiogenic isotopes in rejuvenated-stage lavas from Niihau, Hawaii. *Geochemistry, Geophysics, Geosystems* **9**, 1–34, https://doi.org/10.1029/2008GC002076.

Dixon JE, Clague DA, Wallace P and Poreda R (1997) Volatiles in alkalic basalts form the North Arch volcanic field, Hawaii: extensive degassing of deep submarine-erupted alkalic series lavas. *Journal of Petrology* **38**, 911–39.

Dobson DP, Jones AP, Rabe R, Sekine T, Kurita K, Taniguchi T, Kondo T, Kato T, Shimomura O and Urakawa S (1996) In-situ measurement of viscosity and density of carbonate melts at high pressure. *Earth and Planetary Science Letters* **143**, 207–15.

Doucet LS, Peslier AH, Ionov DA, Brandon AD, Golovin AV, Goncharov AG and Ashchepkov IV (2014) High water contents in the siberian cratonic mantle linked to metasomatism: an FTIR study of Udachnaya peridotite xenoliths. *Geochimica et Cosmochimica Acta* **137**, 159–87, https://doi.org/10.1016/j.gca.2014.04.011.

Evans P (1964) The tectonic framework of Assam. *Journal of Geological Society of India* **5**, 80–96.

Frezzotti ML, Tecce F and Casagli A (2012) Raman spectroscopy for fluid inclusion analysis. *Journal of Geochemical Exploration* **112**, 1–20, https://doi.org/10.1016/j.gexplo.2011.09.009.

Gervasoni F, Klemme S, Rohrbach A, Grützner T and Berndt J (2017) Experimental constraints on mantle metasomatism caused by silicate and carbonate melts. *Lithos* **282**, 173–86.

Grassi D and Schmidt MW (2011) The melting of carbonated pelites from 70 to 700 km depth. *Journal of Petrology* **52**, 765–89.

Green DH and Wallace ME (1988) Mantle metasomatism by ephemeral carbonatite melts. *Nature* **336**, 459.

Gupta RP and Sen AK (1988) Imprints of the Ninety-East Ridge in the Shillong Plateau, Indian Shield. *Tectonophysics* **154**, 335–41, https://doi.org/10.1016/0040-1951(88)90111-4.

Hammouda T and Laporte D (2000) Ultrafast mantle impregnation by carbonatite melts. *Geology* **28**, 283–5.

Harmer RE (1999) The petrogenetic association of carbonatite and alkaline magmatism: constraints from the Spitskop Complex, South Africa. *Journal of Petrology* **40**, 525–48, https://doi.org/10.1093/petroj/40.4.525.

Hauri EH, Shimizu N, Dieu JJ and Hart SR (1993) Evidence for hotspot-related carbonatite metasomatism in the oceanic upper mantle. *Nature* **365**, 221.

Ionov DA, Dupuy C, O'Reilly SY, Kopylova MG and Genshaft YS (1993) Carbonated peridotite xenoliths from Spitsbergen: implications for trace element signature of mantle carbonate metasomatism. *Earth and Planetary Science Letters* **119**, 283–97, https://doi.org/10.1016/0012-821X(93)90139-Z.

Jones AP, Genge M and Carmody L (2013) Carbonate melts and carbonatites. *Reviews in Mineralogy and Geochemistry* **75**, 289–322.

https://doi.org/10.1017/S0016756820000631 Published online by Cambridge University Press

Kelemen PB and Matter J (2008) In situ carbonation of peridotite for CO_2 storage. *Proceedings of the National Academy of Sciences* **105**, 17295–300, https://doi.org/10.1073/pnas.0805794105.

Keller J and Hoefs J (1995) Stable isotope characteristics of recent natrocarbonatite from Oldoiyno Lengai. In *Carbonatite Volcanism: Oldoinyo Lengai and Petrogenesis of Natrocarbonatite* (eds K Bell and J Keller), pp. 113–23. Berlin: Springer.

Kogarko L, Kurat G and Ntaflos T (2001) Carbonate metasomatism of the oceanic mantle beneath Fernando de Noronha Island, Brazil. *Contributions to Mineralogy and Petrology* **140**, 577–87, https://doi.org/10.1007/s004100000201.

Kwak JH, Hu JZ, Turcu RV, Rosso KM, Ilton ES, Wang C, Sears JA, Engelhard MH, Felmy AR and Hoyt DW (2011) The role of H_2O in the carbonation of forsterite in supercritical CO_2. *International Journal of Greenhouse Gas Control* **5**, 1081–92, https://doi.org/10.1016/j.ijggc.2011.05.013.

Kyser TK (1990) Stable isotopes in the continental lithospheric mantle. In *The Continental Lithosphere* (ed. M Menzies), pp. 127–56. Oxford: Oxford University Press.

Lee WJ and Wyllie PJ (1998) Petrogenesis of carbonatite magmas from mantle to crust, constrained by the system CaO–(MgO+ FeO*)–(Na2O+ K2O)–(SiO2+ Al2O3+ TiO2)-CO2. *Journal of Petrology* **39**, 495–517.

Loring JS, Chen J, Bénézeth P, Qafoku O, Ilton ES, Washton NM, Thompson CJ, Martin PF, McGrail BP, Rosso KM and Felmy AR (2015) Evidence for carbonate surface complexation during forsterite carbonation in wet supercritical carbon dioxide. *Langmuir* **31**, 7533–43, https://doi.org/10.1021/acs.langmuir.5b01052.

Melluso L, Srivastava RK, Guarino V, Zanetti A and Sinha AK (2010) Mineral compositions and petrogenetic evolution of the Ultramafic-Alkaline-Carbonatite complex of Sung Valley, Northeastern India. *The Canadian Mineralogist* **48**, 205–29. https://doi.org/10.3749/canmin.48.1.205.

Mitchell RH (2005) Carbonatites and carbonatites and carbonatites. *The Canadian Mineralogist* **43**, 2049–68.

Nandy DR (1980) Tectonic pattern in Northeastern India. *Indian Journal of Earth Science* **7**, 103–7.

O'Reilly SY and Griffin WL (2013) Mantle metasomatism. In *Metasomatism and the Chemical Transformation of Rock* (eds DE Harlov and H Austrheim), pp. 471–533. Berlin, Heidelberg: Springer.

Pearson DG and Wittig N (2014) The formation and evolution of cratonic mantle lithosphere evidence from mantle xenoliths. In *Reference Module in Earth Systems and Environmental Sciences* (eds HD Holland and KK Turekian), pp. 255–92. Amsterdam: Elsevier, Treatise on Geochemistry.

Pokhilenko NP, Agashev AM, Litasov KD and Pokhilenko LN (2015) Carbonatite metasomatism of peridotite lithospheric mantle: implications for diamond formation and carbonatite-kimberlite magmatism. *Russian Geology and Geophysics* **56**, 280–95, http://dx.doi.org/10.1016/j.rgg.201.0.020.

Ray JS and Pande K (2001) ^{40}Ar-^{39}Ar age of carbonatite-alkaline magmatism in Sung Valley, Meghalaya, India. *Journal of Earth System Science* **110**, 185–90, https://doi.org/10.1007/BF02702233.

Ray JS and Ramesh R (2000) Rayleigh fractionation of stable isotopes from a multicomponent source. *Geochimica et Cosmochimica Acta* **64**, 299–306.

Ray JS and Ramesh R (2006) Stable carbon and oxygen isotopic compositions of Indian Carbonatites. *International Geology Review* **48**, 17–45.

Ray JS, Ramesh R and Pande K (1999) Carbon isotopes in Kerguelen Plume-derived carbonatites: evidence for recycled inorganic carbon. *Earth and Planetary Science Letters* **170**, 205–14.

Ray JS, Trivedi JR and Dayal AM (2000) Strontium isotope systematics of Amba Dongar and Sung Valley carbonatite-alkaline complexes, India: evidence for liquid immiscibility, crustal contamination and long-lived Rb/Sr enriched mantle sources. *Journal of Asian Earth Sciences* **18**, 585–94.

Roedder E (1984) Fluid inclusions, reviews in mineralogy. *Geochimica et Cosmochimica Acta* **49**(6), 1491, https://doi.org/10.1016/0016-7037(85)90299-6.

Rudnick RL, McDonough WF and Chappell BW (1993) Carbonatite metasomatism in the Northern Tanzanian mantle: petrographic and geochemical characteristics. *Earth and Planetary Science Letters* **114**, 463–75, https://doi.org/10.1016/0012-821X(93)90076-L.

Sadik M, Ranjith A and Umrao AK (2014) REE mineralization in the carbonatites of the Sung Valley ultramafic-alkaline-carbonatite complex, Meghalaya, India. *Open Geosciences* **6**, 457–75, https://doi.org/10.2478/s13533-012-0191-y.

Sai VS and Sengupta SK (2017) Resorbed forsterite in the carbonatite from the Cretaceous Sung Valley Complex, Meghalaya, NE India–Implications for crystal-melt interaction from textural studies. *Journal of Indian Geophysical Union* **21**, 292–7.

Santrock J, Studley SA and Hayes J (1985) Isotopic analyses based on the mass spectra of carbon dioxide. *Analytical Chemistry* **57**, 1444–8.

Sheppard SME and Dawon JB (1973) ^{13}C/^{12}C and D/H isotope variations in primary igneous carbonatites, Fortschr. *Mineral* **50**, 128–9.

Sokol AG, Kruk AN, Chebotarev DA and Palyanov YN (2016) Carbonatite melt-peridotite interaction at 5.5–7.0 GPa: implications for metasomatism in lithospheric mantle. *Lithos* **248–51**, 66–79.

Spargo SRW (2007) *The Pupuke Volcanic Centre, Polygenetic Magmas in a Mono-genetic Field*. Auckland: University of Auckland, 141 p.

Srivastava RK (1997) Petrology, geochemistry and genesis of rift-related carbonatites of Ambadungar, India. *Mineralogy and Petrology* **61**, 47–66.

Srivastava RK (2020) Early Cretaceous alkaline/ultra-alkaline silicate and carbonatite magmatism in the Indian Shield–a review: implications for a possible remnant of the Greater Kerguelen Large Igneous Province. *Episodes Journal of International Geoscience* **43**, 300–11.

Srivastava RK, Guarino V, Wu FY, Melluso L and Sinha AK (2019) Evidence of sub-continental lithospheric mantle sources and open-system crystallization processes from in-situ U–Pb ages and Nd–Sr–Hf isotope geochemistry of the Cretaceous ultramafic-alkaline (carbonatite) intrusions from the Shillong Plateau, North-Eastern India. *Lithos* **330**, 108–19, https://doi.org/10.1016/j.lithos.2019.02.009.

Srivastava RK and Hall RP (1995) Tectonic setting of Indian carbonatites. In *Magmatism in Relation to Diverse Tectonic Setting* (eds RK Srivastava and R Chandra), pp. 134–54. Rotterdam: AA Balkema.

Srivastava RK, Heaman LM, Sinha AK and Shihua S (2005) Emplacement age and isotope geochemistry of Sung Valley alkaline-carbonatite complex, Shillong Plateau, Northeastern India: implications for primary carbonate melt and genesis of the associated silicate rocks. *Lithos* **81**, 33–54.

Srivastava RK and Sinha AK (2004) Early Cretaceous Sung Valley ultramafic-alkaline-carbonatite complex, Shillong Plateau, Northeastern India: petrological and genetic significance. *Mineralogy and Petrology* **80**, 241–63.

Stopic S, Dertmann C, Modolo G, Kegler P, Neumeier S, Kremer D, Wotruba H, Etzold S, Telle R, Rosani D and Knops P (2018) Synthesis of magnesium carbonate via carbonation under high pressure in an autoclave. *Metals* **8**, 993.

Su B, Chen Y, Guo S, Chu ZY, Liu JB and Gao YJ (2016) Carbonatitic metasomatism in orogenic dunites from Lijiatun in the Sulu UHP Terrane, Eastern China. *Lithos* **262**, 266–84.

Taylor HP, Frechen J and Degens ET (1967) Oxygen and carbon isotopes studies of carbonatites from the Laacher Sea district, West Germany and the Alno districts, Sweden. *Geochimica et Cosmochimica Acta* **31**, 407–30.

Todd Schaef H, McGrail BP, Loring JL, Bowden ME, Arey BW and Rosso KM (2013) Forsterite [Mg_2SiO_4] carbonation in wet supercritical CO_2: an in situ high-pressure X-ray diffraction study. *Environmental Science & Technology* **47**, 174–81.

Veena K, Pandey BK, Krishnamurthy P and Gupta JN (1998) Pb, Sr and Nd isotopic systematics of the carbonatites of Sung Valley, Meghalaya, Northeast India: implications for contemporary plume-related mantle source characteristics. *Journal of Petrology* **39**, 1875–84, https://doi.org/10.1093/petroj/39.11-12.1875.

Woolley AR and Kemp DRC (1989) Carbonatites: nomenclature, average chemical compositions and element distribution. In *Carbonatites Genesis and Evolution* (ed K Bell), pp. 1–14. London: Unwin Hyman.

Woolley AR, Barr MWC, Din VK, Jones GC, Wall F and Williams CT (1991) Extrusive carbonatites from the Uyaynah Area, United Arab Emirates. *Journal of Petrology* **32**, 1143–67, https://doi.org/10.1093/petrology/32.6.1143.

https://doi.org/10.1017/S0016756820000631 Published online by Cambridge University Press

Xiong W and Giammar D (2014) Forsterite carbonation in zones with transport limited by diffusion. *Environmental Science & Technology Letters* **1**, 333–8, https://doi.org/10.1021/ez500182s.

Yaxley GM (1993) Carbonatite metasomatism in the mantle: sources and roles of carbonate in metasomatic enrichment processes in the lithosphere. Ph.D. thesis, University of Tasmania. Published thesis.

Yaxley GM, Crawford AJ and Green DH (1991) Evidence for carbonatite metasomatism in spinel peridotite xenoliths from Western Victoria, Australia. *Earth and Planetary Science Letters* **107**, 305–17, https://doi.org/10.1016/0012-821X(91)90078-V.

Yaxley GM, Green DH and Kamenetsky V (1998) Carbonatite metasomatism in the southeastern Australian lithosphere. *Journal of Petrology* **39**, 1917–30.

https://doi.org/10.1017/S0016756820000631 Published online by Cambridge University Press